
High-Order Pooling for Graph Neural Networks with Tensor Decomposition

Chenqing Hua^{1,4*} Guillaume Rabusseau^{2,4,5,6} Jian Tang^{3,4,6}
¹McGill University; ²Université de Montréal; ³HEC Montréal;
⁴Mila; ⁵DIRO; ⁶CIFAR AI Chair

Abstract

Graph Neural Networks (GNNs) are attracting growing attention due to their effectiveness and flexibility in modeling a variety of graph-structured data. Existing GNN architectures usually adopt simple pooling operations (*e.g.*, sum, average, max) when aggregating messages from a local neighborhood for updating node representation or pooling node representations from the entire graph to compute the graph representation. Though simple and effective, these linear operations do not model high-order non-linear interactions among nodes. We propose the Tensorized Graph Neural Network (tGNN), a highly expressive GNN architecture relying on tensor decomposition to model high-order non-linear node interactions. tGNN leverages the symmetric CP decomposition to efficiently parameterize permutation-invariant multilinear maps for modeling node interactions. Theoretical and empirical analysis on both node and graph classification tasks show the superiority of tGNN over competitive baselines. In particular, tGNN achieves the most solid results on two OGB node classification datasets and one OGB graph classification dataset.

1 Introduction

Graph neural networks (GNNs) generalize traditional neural network architectures for data in the Euclidean domain to data in non-Euclidean domains [26, 45, 34, 35]. As graphs are very general and flexible data structures and are ubiquitous in the real world, GNNs are now widely used in a variety of domains and applications such as social network analysis [20], recommender systems [49], graph reasoning [55], and drug discovery [42].

Indeed, many GNN architectures (*e.g.*, GCN [26], GAT [45], MPNN [16]) have been proposed. The essential idea of all these architectures is to iteratively update node representations by aggregating the information from their neighbors through multiple rounds of neural message passing. The final node representations can be used for downstream tasks such as node classification or link prediction. For graph classification, an additional readout layer is used to combine all the node representations to calculate the entire graph representation. In general, an effective aggregation (or pooling) function is required to aggregate the information at the level of both local neighborhoods and the entire graph. In practice, some simple aggregation functions are usually used such as sum, mean, and max. Though simple and effective in some applications, the expressiveness of these functions is limited as they only model linear combinations of node features, which can limit their effectiveness in some cases.

A recent work, principled neighborhood aggregation (PNA) [13], aims to design a more flexible aggregation function by combining multiple simple aggregation functions, each of which is associated with a learnable weight. However, the practical capacity of PNA is still limited by simply combining multiple *simple* aggregation functions. A more expressive solution would be to model high-order non-linear interactions when aggregating node features. However, explicitly modeling high-order

*Correspondence to: Chenqing Hua <chenqing.hua@mail.mcgill.ca>

non-linear interactions among nodes is very expensive, with both the time and memory complexity being exponential in the size of the neighborhood. This raises the question of whether there exists an aggregation function which can model high-order non-linear interactions among nodes while remaining computationally efficient.

In this paper, we propose such an approach based on symmetric tensor decomposition. We design an aggregation function over a set of node representations for graph neural networks, which is permutation-invariant and is capable of modeling non-linear high-order multiplicative interactions among nodes. We leverage the symmetric CANDECOMP/PARAFAC decomposition (CP) [22, 29] to design an efficient parameterization of permutation-invariant multilinear maps over a set of node representations. Theoretically, we show that the CP layer can compute any permutation-invariant multilinear polynomial, including the classical sum and mean aggregation functions. We also show that the CP layer is universally strictly more expressive than sum and mean pooling: with probability one, any function computed by a random CP layer cannot be computed using sum and mean pooling.

We propose the CP-layer as an expressive mean of performing the aggregation and update functions in GNN. We call the resulting model a *tensorized GNN* (tGNN). We evaluate tGNN on both node and graph classification tasks. Experimental results on real-world large-scale datasets show that our proposed architecture outperforms or can compete with existing state-of-the-art approaches and traditional pooling techniques. Notably, our proposed method is more effective and expressive than existing GNN architectures and pooling methods on two citation networks, two *OGB* node datasets, and one *OGB* graph dataset.

Summary of Contributions We propose a new aggregation layer, the CP layer, for pooling and readout functions in GNNs. This new layer leverages the symmetric CP decomposition to efficiently parameterize polynomial maps, thus taking into account high-order multiplicative interactions between node features. We theoretically show that the CP layer can compute any permutation-invariant multilinear polynomial including sum and mean pooling. Using the CP layer as a drop-in replacement for sum pooling in classical GNN architectures, our approach achieves more effective and expressive results than existing GNN architectures and pooling methods on several benchmark graph datasets.

2 Preliminaries

2.1 Notation

We use bold font letters for vectors (*e.g.*, \mathbf{v}), capital letters (*e.g.*, \mathbf{M} , \mathcal{T}) for matrices and tensors respectively, and regular letters for nodes (*e.g.*, v). Let $G = (V, E)$ be a graph, where V is the node set and E is the edge set with self-loop. We use $N(v)$ to denote the neighborhood set of node v , *i.e.*, $N(v) = \{u : e_{vu} \in E\}$. A node feature is a vector $\mathbf{x} \in \mathbb{R}^F$ defined on V , where \mathbf{x}_v is defined on the node v . We use \otimes to denote the Kronecker product, \circ to denote the outer product, and \odot to denote the Hadamard (*i.e.*, component-wise) product between vectors, matrices, and tensors. For any integer k , we use the notation $[k] = \{1, \dots, k\}$.

2.2 Tensors

We introduce basic notions of tensor algebra, more details can be found in [29]. A k -th order tensor $\mathcal{T} \in \mathbb{R}^{N_1 \times N_2 \times \dots \times N_k}$ can simply be seen as a multidimensional array. The mode- i fibers of \mathcal{T} are the vectors obtained by fixing all indices except the i -th one: $\mathcal{T}_{n_1, n_2, \dots, n_{i-1}, :, n_{i+1}, \dots, n_k} \in \mathbb{R}^{N_i}$. The i -th mode matricization of a tensor is the matrix having its mode- i fibers as columns and is denoted by $\mathcal{T}_{(i)}$, *e.g.*, $\mathcal{T}_{(1)} \in \mathbb{R}^{N_1 \times N_2 \dots N_k}$. We use $\mathcal{T} \times_i \mathbf{v} \in \mathbb{R}^{N_1 \times \dots \times N_{i-1} \times N_{i+1} \times \dots \times N_k}$ to denote the mode- i product between a tensor $\mathcal{T} \in \mathbb{R}^{N_1 \times \dots \times N_k}$ and a vector $\mathbf{v} \in \mathbb{R}^{N_i}$, which is defined by $(\mathcal{T} \times_i \mathbf{v})_{n_1, \dots, n_{i-1}, n_{i+1}, \dots, n_k} = \sum_{n_i=1}^{N_i} \mathcal{T}_{n_1, \dots, n_k} \mathbf{v}_{n_i}$. The following useful identity relates the mode- i product with the Kronecker product:

$$\mathcal{T} \times_1 \mathbf{v}_1 \times_2 \dots \times_{k-1} \mathbf{v}_{k-1} = \mathcal{T}_{(k)} (\mathbf{v}_{k-1} \otimes \dots \otimes \mathbf{v}_1). \quad (1)$$

2.3 CANDECOMP/PARAFAC Decomposition

We refer to CANDECOMP/PARAFAC decomposition of a tensor as CP decomposition [24, 22]. A Rank R CP decomposition factorizes a k -th order tensor $\mathcal{T} \in \mathbb{R}^{N_1 \times \dots \times N_k}$ into the sum of R

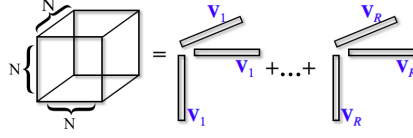


Figure 1: Example of a rank R symmetric CP decomposition of a symmetric 3-order tensor $\mathcal{T} \in \mathbb{R}^{N \times N \times N}$ such that $\mathcal{T} = \sum_{r=1}^R \mathbf{v}_r \circ \mathbf{v}_r \circ \mathbf{v}_r$.

rank one tensors as $\mathcal{T} = \sum_{r=1}^R \mathbf{v}_{1r} \circ \mathbf{v}_{2r} \circ \dots \circ \mathbf{v}_{kr}$, where \circ denotes the vector outer-product and $\mathbf{v}_{1r} \in \mathbb{R}^{N_1}$, $\mathbf{v}_{2r} \in \mathbb{R}^{N_2}$, \dots , $\mathbf{v}_{kr} \in \mathbb{R}^{N_k}$ for every $r = 1, 2, \dots, R$.

The decomposition vectors, $\mathbf{v}_{:r}$ for $r = 1, \dots, R$, are equal in length, thus can be naturally gathered into factor matrices $\mathbf{M}_1 = [\mathbf{v}_{11}, \dots, \mathbf{v}_{1R}] \in \mathbb{R}^{N_1 \times R}$, \dots , $\mathbf{M}_k = [\mathbf{v}_{k1}, \dots, \mathbf{v}_{kR}] \in \mathbb{R}^{N_k \times R}$. Using the factor matrices, we denote the CP decomposition of \mathcal{T} as

$$\mathcal{T} = \sum_{r=1}^R \mathbf{v}_{1r} \circ \mathbf{v}_{2r} \circ \dots \circ \mathbf{v}_{kr} = \llbracket \mathbf{M}_1, \mathbf{M}_2, \dots, \mathbf{M}_k \rrbracket.$$

The k -th order tensor \mathcal{T} is *cubical* if all its modes have the same size, *i.e.*, $N_1 = N_2 = \dots = N_k := N$. A tensor \mathcal{T} is symmetric if it is cubical and is invariant under permutation of its indices:

$$\mathcal{T}_{n_{\phi(1)}, \dots, n_{\phi(k)}} = \mathcal{T}_{n_1, \dots, n_k}, \quad n_1, \dots, n_k \in [N]$$

for any permutation $\phi: [k] \rightarrow [k]$. A rank R symmetric CP decomposition of a symmetric tensor \mathcal{T} is a decomposition of the form $\mathcal{T} = \llbracket \mathbf{M}, \dots, \mathbf{M} \rrbracket$ with $\mathbf{M} \in \mathbb{R}^{N \times R}$. It is well known that any symmetric tensor admits a symmetric CP decomposition [12], we illustrate a rank R symmetric CP decomposition in Fig. 1.

We say that a tensor \mathcal{T} is partially symmetric if it is symmetric in a subset of its modes [28]. For example, a 3-rd order tensor $\mathcal{T} \in \mathbb{R}^{N_1 \times N_1 \times N_3}$ is partially symmetric w.r.t. modes 1 and 2 if it has symmetric frontal slices; *i.e.*, $\mathcal{T}_{:, :, k}$ is a symmetric matrix for all $k \in [N_3]$. We prove the fact that any partially symmetric tensor admits a partially symmetric CP decomposition in Lemma 1 in Appendix A, *e.g.*, if $\mathcal{T} \in \mathbb{R}^{N_1 \times N_1 \times N_3}$ is partially symmetric w.r.t. modes 1 and 2, there exist $\mathbf{M} \in \mathbb{R}^{N_1 \times R}$ and $\mathbf{W} \in \mathbb{R}^{N_3 \times R}$ such that $\mathcal{T} = \llbracket \mathbf{M}, \mathbf{M}, \mathbf{W} \rrbracket$.

2.4 Graph Neural Networks and Pooling Functions

Given a graph $G = (V, E)$, a graph neural network always aggregates information in a neighborhood to give node-level representations. During each message-passing iteration, the embedding \mathbf{h}_v corresponding to node $v \in V$ is generated by aggregating features from $N(v)$ [18]. Formally, at the l -th layer of a graph neural network,

$$\mathbf{m}_{N(v)}^{(l)} = \text{AGGREGATE}^{(l)}(\{\mathbf{h}_u^{(l-1)}, \forall u \in N(v)\}), \quad \mathbf{h}_v^{(l)} = \text{UPDATE}^{(l)}(\mathbf{h}_v^{(l-1)}, \mathbf{m}_{N(v)}^{(l)}), \quad (2)$$

where $\text{AGGREGATE}^{(l)}(\cdot)$ and $\text{UPDATE}^{(l)}(\cdot)$ are differentiable functions, the former being permutation-invariant. In words, $\text{AGGREGATE}^{(l)}(\cdot)$ first aggregates information from $N(v)$, then $\text{UPDATE}^{(l)}(\cdot)$ combines the aggregated message and previous node embedding $\mathbf{h}_v^{(l-1)}$ to give a new embedding.

The node representation $\mathbf{h}_v^{(L)}$ of node v from the last GNN layer L can be used for predicting relevant properties of the node. For graph classification, an additional $\text{READOUT}(\cdot)$ function aggregates node representations from the final layer to obtain a graph representation \mathbf{h}_G of graph G as,

$$\mathbf{h}_G = \text{READOUT}(\{\mathbf{h}_v^{(L)} | v \in V\}), \quad (3)$$

where $\text{READOUT}(\cdot)$ can be a simple permutation-invariant function (*e.g.*, sum, mean, *etc.*) or a more sophisticated graph pooling function [50, 48].

In the general design of GNNs, it is important to have an effective pooling function to aggregate messages from local neighborhoods and update node representations (see Eq. equation 2), and to combine node representations to compute a representation at the graph level (see Eq. equation 3).

3 Meaning of High-Order of tGNN

In our paper, high-order refers to multi-dimensional feature products between nodes in a neighborhood. [38, 43] are previous works on high-dimensional feature products, and introduce how to use tensor methods to achieve those products. They have stated the importance of having high-order products in physics and geometries. For example, if we have x_1 and x_2 , a simple GNN layer can result in a vector of $[x_1, x_2, x_1 + x_2]$, but our high-order layer result in a vector of $[x_1, x_2, x_1 + x_2, x_1x_2]$ with another term x_1x_2 . And if we have we have x_1, x_2 , and x_3 , a simple low-order GNN layer will result in $[x_1, x_2, x_3, x_1 + x_2, x_1 + x_3, x_2 + x_3, x_1 + x_2 + x_3]$ while the high-order layer will result in a vector of $[x_1, x_2, x_3, x_1 + x_2, x_1 + x_3, x_2 + x_3, x_1 + x_2 + x_3, x_1x_2, x_1x_3, x_2x_3, x_1x_2x_3]$ with extra 4 terms at a higher feature dimension. In general content of GNNs, high-order will normally refer to the ability of capturing long-range dependencies, the interactions between long-range nodes [48, 2, 46], but ours refers to the multi-dimensional node feature products. However, the CP layer is able to capture stacking long-range dependencies by stacking layers like other simple GNNs [26, 45].

One may raise a question on why we need to compute multi-dimensional feature products. The idea is fairly easy if one thinks the multi-dimensional feature space. Take a molecular graph dataset as an example, and blood pressure could be one feature. Many studies analyze the impact of blood pressure on one’s health. Blood pressure is the feature in this case. So, one could try to predict life expectancy using blood pressure as a feature, but you can imagine that this might not be sufficient. You really need more information. So you could add age, exercise frequency, and body fat to see if you can predict a person’s life expectancy. Those additional measurements are also features and now every individual has a multi-dimensional feature vector consisting of these measurements. However, a simple GNN with one-dimensional feature interactions may not capture the correlation between age, exercise frequency, and body fat. There could be some correlation between the three factors to predict life expectancy. A simple GNN that does age+exercise frequency+body fat is not able to capture the correlation between those factors. Still, our multi-dimensional feature product can capture age×exercise frequency, age×body fat, exercise frequency×body fat, age×exercise frequency×body fat, all the correlations to predict life expectancy. So in molecular graph case, high-dimensional feature products are importantly needed to make a prediction as most features are correlated (like in atom graphs, atom charge, and atom mass), and our model shows some significant improvements on molecular datasets in Sec.6. And the high-dimensional feature products might also be important for other networks and applications [38, 43].

4 Tensorized Graph Neural Network

In this section, we introduce the CP-layer and tensorized GNNs (tGNN). For convenience, we let $\{\mathbf{x}_1, \mathbf{x}_2, \dots, \mathbf{x}_k\}$ denote features of a node v and its 1-hop neighbors $N(v)$ such that $|\{v\} \cup N(v)| = k$.

4.1 Motivation and Method

We leverage the symmetric CP decomposition to design an efficient parameterization of permutation-invariant multilinear maps for aggregation operations in graph neural networks, Tensorized Graph Neural Network (tGNN), resulting in a more expressive high-order node interaction scheme. We visualize the CP pooling layer and compare it with sum pooling in Fig. 2.

Let $\mathcal{T} \in \mathbb{R}^{N \times N \times \dots \times N \times M}$ of order $k + 1$ be a tensor which is partially symmetric w.r.t. its first k modes. We can parameterize \mathcal{T} using a rank R partially symmetric CP decomposition (see Section 2.3): $\mathcal{T} = \llbracket \mathbf{W}, \dots, \mathbf{W}, \mathbf{M} \rrbracket$ where $\mathbf{W} \in \mathbb{R}^{N \times R}$ and $\mathbf{M} \in \mathbb{R}^{M \times R}$. Such a tensor naturally defines a map from $(\mathbb{R}^N)^k$ to \mathbb{R}^M using contractions over the first k modes:

$$f(\mathbf{x}_1, \dots, \mathbf{x}_k) = \mathcal{T} \times_1 \mathbf{x}_1 \times_2 \dots \times_k \mathbf{x}_k = \underbrace{\llbracket \mathbf{W}, \dots, \mathbf{W}, \mathbf{M} \rrbracket}_{k \text{ times}} \times_1 \mathbf{x}_1 \times_2 \dots \times_k \mathbf{x}_k. \quad (4)$$

This map satisfies two very important properties for GNNs: it is *permutation-invariant* (due to the partial symmetry of \mathcal{T}) and *its number of parameters is independent of k* (due to the partially symmetric CP parameterization). Thus, using only two parameter matrices of fixed size, the map in Eq. equation 4 can be applied to sets of N -dimensional vectors of arbitrary cardinality. In particular, we will show that it can be leveraged to replace both the AGGREGATE and UPDATE functions in GNNs.

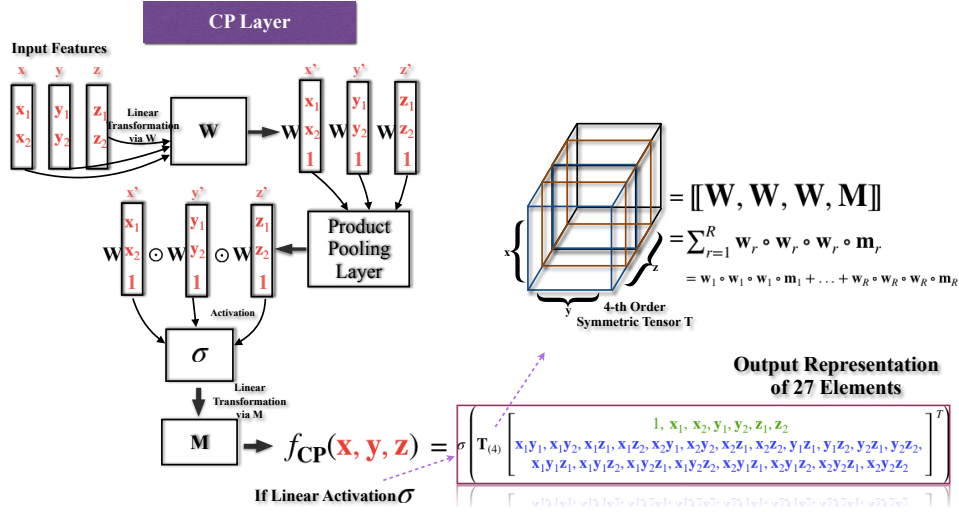


Figure 2: (Left) Sum pooling followed by a FC layer: the output takes individual components of the input into account. (Right) The CP layer can be interpreted as a combination of product pooling with linear layers (with weight matrices \mathbf{W} and \mathbf{M}) and non-linearities. The weight matrices of a CP layer corresponds to a partially symmetric CP decomposition of a weight tensor $\mathcal{T} = \llbracket \mathbf{W}, \mathbf{W}, \mathbf{W}, \mathbf{M} \rrbracket$. It shows that the output of a CP layer takes high-order multiplicative interactions of the inputs' components into account (in contrast with sum pooling that only considers 1st order terms).

There are several way to interpret the map in Eq. equation 4. First, from Eq. equation 1 we have

$$f(\mathbf{x}_1, \dots, \mathbf{x}_k) = \mathcal{T} \times_1 \mathbf{x}_1 \times_2 \dots \times_k \mathbf{x}_k = \mathcal{T}_{(k+1)}(\mathbf{x}_k \otimes \mathbf{x}_{k-1} \otimes \dots \otimes \mathbf{x}_1),$$

where $\mathcal{T}_{(k+1)} \in \mathbb{R}^{M \times N^k}$ is the mode- $(k+1)$ matricization of \mathcal{T} . This shows that each element of the output $f(\mathbf{x}_1, \dots, \mathbf{x}_k)$ is a linear combinations of terms of the form $(\mathbf{x}_1)_{i_1} (\mathbf{x}_2)_{i_2} \dots (\mathbf{x}_k)_{i_k}$ (k -th order multiplicative interactions between the components of the vectors $\mathbf{x}_1, \dots, \mathbf{x}_k$). That is, f is a multivariate polynomial map of order k involving only k -th order interactions. By using homogeneous coordinates, *i.e.*, appending an entry equal to one to each of the input tensors \mathbf{x}_i , the map f becomes a more general polynomial map taking into account all multiplicative interactions between the \mathbf{x}_i up to the k -th order:

$$f(\mathbf{x}_1, \dots, \mathbf{x}_k) = \mathcal{T} \times_1 \begin{bmatrix} \mathbf{x}_k \\ 1 \end{bmatrix} \times_2 \dots \times_k \begin{bmatrix} \mathbf{x}_1 \\ 1 \end{bmatrix} = \mathcal{T}_{(k+1)} \left(\begin{bmatrix} \mathbf{x}_k \\ 1 \end{bmatrix} \otimes \dots \otimes \begin{bmatrix} \mathbf{x}_1 \\ 1 \end{bmatrix} \right)$$

where \mathcal{T} is now of size $(N+1) \times \dots \times (N+1) \times M$ and can still be parameterized using the partially symmetric CP decomposition $\mathcal{T} = \llbracket \mathbf{W}, \dots, \mathbf{W}, \mathbf{M} \rrbracket$ with $\mathbf{W} \in \mathbb{R}^{(N+1) \times R}$ and $\mathbf{M} \in \mathbb{R}^{M \times R}$. With this parameterization, one can check that

$$f(\mathbf{x}_1, \dots, \mathbf{x}_k) = \mathbf{M} \left(\left(\mathbf{W}^\top \begin{bmatrix} \mathbf{x}_1 \\ 1 \end{bmatrix} \right) \odot \dots \odot \left(\mathbf{W}^\top \begin{bmatrix} \mathbf{x}_k \\ 1 \end{bmatrix} \right) \right)$$

where \odot denotes the component-wise product between vectors. The map f can thus be seen as the composition of a linear layer with weight \mathbf{W} , a multiplicative pooling layer, and another linear map \mathbf{M} . Since it is permutation-invariant and can be applied to any number of input vectors, this map can be used as both the aggregation, update, and readout functions of a GNN using non-linear activation functions, which leads us to introduce the novel *CP layer* for GNN.

Definition 1. (*CP layer*) Given parameter matrices $\mathbf{M} \in \mathbb{R}^{d \times R}$ and $\mathbf{W} \in \mathbb{R}^{F+1 \times R}$ and activation functions σ, σ' , a rank R CP layer computes the function $f_{CP} : \cup_{i \geq 1} (\mathbb{R}^F)^i \rightarrow \mathbb{R}^d$ defined by

$$f_{CP}(\mathbf{x}_1, \dots, \mathbf{x}_k) = \sigma' \left(\mathbf{M} \left(\sigma \left(\mathbf{W}^\top \begin{bmatrix} \mathbf{x}_1 \\ 1 \end{bmatrix} \odot \dots \odot \mathbf{W}^\top \begin{bmatrix} \mathbf{x}_k \\ 1 \end{bmatrix} \right) \right) \right)$$

for any $k \geq 1$ and any $\mathbf{x}_1, \dots, \mathbf{x}_k \in \mathbb{R}^F$.

The rank R of a CP layer is a hyperparameter controlling the trade-off between parameter efficiency and expressiveness. Note that the CP layer computes AGGREGATE and UPDATE (see Eq. 2) in one step. One can think of the component-wise product of the $\mathbf{W}^\top [\mathbf{x}_i \ 1]^\top$ as AGGREGATE, while

the UPDATE corresponds to the two non-linear activation functions and linear transformation \mathbf{M} . We observed in our experiments that the non-linearity σ is crucial to avoid numerical instabilities during training caused by repeated products of \mathbf{W} . In practice, we use *Tanh* for σ and *ReLU* for σ' . Fig. 2 graphically explains the computational process of a CP layer, comparing it with a classical sum pooling operation. We intuitively see in this figure that the CP layer is able to capture high order multiplicative interactions that are not modeled by simple aggregation functions such as the sum or the mean. In the next section, we theoretically formalize this intuition.

Complexity Analysis The sum, mean and max poolings result in $O(F_{in}(N + F_{out}))$ time complexity, while CP pooling is $O(R(NF_{in} + F_{out}))$, where N denotes the number of nodes, F_{in} is the input feature dimension, F_{out} is out feature dimension, and R is the CP decomposition rank. In Sec. 6.3, we experimentally compare tGNN and CP pooling with various GNNs and pooling techniques to show the model efficiency with limited computation and time budgets.

4.2 Theoretical Analysis

We now analyze the expressive power of CP layers. In order to characterize the set of functions that can be computed by CP layers, we first introduce the notion of multilinear polynomial. A multilinear polynomial is a special kind of vector-valued multivariate polynomial in which no variables appears with a power of 2 or higher. More formally, we have the following definition.

Definition 2. A function $g : \mathbb{R}^k \rightarrow \mathbb{R}$ is called a univariate multilinear polynomial if it can be written as

$$g(a_1, a_2, \dots, a_k) = \sum_{i_1=0}^1 \dots \sum_{i_k=0}^1 \tau_{i_1 i_2 \dots i_k} a_1^{i_1} a_2^{i_2} \dots a_k^{i_k}$$

where each $\tau_{i_1 i_2 \dots i_k} \in \mathbb{R}$. The degree of a univariate multilinear polynomial is the maximum number of distinct variables occurring in any of the non-zero monomials $\tau_{i_1 i_2 \dots i_n} a_1^{i_1} a_2^{i_2} \dots a_k^{i_k}$.

A function $f : (\mathbb{R}^d)^k \rightarrow \mathbb{R}^p$ is called a multilinear polynomial map if there exist univariate multilinear polynomials g_{i, j_1, \dots, j_n} for $j_1, \dots, j_k \in [d]$ and $i \in [p]$ such that

$$f(\mathbf{x}_1, \dots, \mathbf{x}_k)_i = \sum_{j_1, \dots, j_k=1}^d g_{i, j_1, \dots, j_k}((\mathbf{x}_1)_{j_1}, \dots, (\mathbf{x}_k)_{j_k})$$

for all $\mathbf{x}_1, \dots, \mathbf{x}_k \in \mathbb{R}^d$ and all $i \in [p]$. The degree of f is the highest degree of the multilinear polynomials g_{i, j_1, \dots, j_k} .

The following theorem shows that CP layers can compute any permutation-invariant multilinear polynomial map. We also visually represent the expressive power of CP layers in Fig. 3, showing that the class of functions computed by CP layer subsumes multilinear polynomials (including sum and mean aggregation functions).

Theorem 1. The function computed by a CP layer (Eq. equation 1) is permutation-invariant. In addition, any permutation-invariant multilinear polynomial $f : (\mathbb{R}^F)^k \rightarrow \mathbb{R}^d$ can be computed by a CP layer (with a linear activation function).

Note also that in Fig. 3 the CP layer is strictly more expressive than permutation invariant multilinear polynomials due to the non-linear activation functions in Def. 1. Since the classical sum and mean pooling aggregation functions are degree 1 multilinear polynomial maps, it readily follows from the previous theorem that the CP layer is more expressive than these standards aggregation functions. However, it is natural to ask how many parameters a CP layer needs to compute sums and means. We answer this question in the following theorem.

Theorem 2. A CP layer of rank $F \cdot k$ can compute the sum and mean aggregation functions over k vectors in \mathbb{R}^F .

Consequently, for any $k \geq 1$ and any GNN \mathcal{N} using mean or sum pooling with feature and embedding dimensions bounded by F , there exists a GNN with CP layers of rank $F \cdot k$ computing the same function as \mathcal{N} over all graphs of uniform degree k .

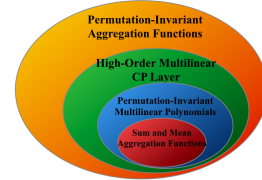


Figure 3: Visualization of relations of $\{\text{permutation-invariant function space}\} \supseteq \{\text{CP function space}\} \supseteq \{\text{permutation-invariant multilinear polynomial space}\} \supseteq \{\text{sum and mean aggregation functions}\}$.

It follows from this theorem that a CP layer with $2F^2k$ can compute sum and mean aggregation over sets of k vectors. While Theorem 2 shows that any function using sum and mean aggregation can be computed by a CP layer, the next theorem shows that the converse is not true, *i.e.*, the CP layer is a strictly more expressive aggregator than using the mean or sum.

Theorem 3. *With probability one, any function $f_{CP} : (\mathbb{R}^F)^k \rightarrow \mathbb{R}^d$ computed by a CP layer (of any rank) whose parameters are drawn randomly (from a distribution which is continuous w.r.t. the Lebesgue measure) cannot be computed by a function of the form*

$$g_{sum} : \mathbf{x}_1, \dots, \mathbf{x}_k \mapsto \sigma' \left(\mathbf{M} \left(\sigma \left(\sum_{i=1}^k \mathbf{W}^\top \mathbf{x}_i \right) \right) \right)$$

where $\mathbf{M} \in \mathbb{R}^{d \times R}$, $\mathbf{W} \in \mathbb{R}^{F \times R}$ and σ, σ' are component-wise activation function.

This theorem not only shows that there exist functions computed by CP layers that cannot be computed using sum pooling, but that this is the case for *almost all* functions that can be computed by (even rank-one) CP layers.

From an expressive power viewpoint, we showed that a CP layer is able to leverage both low and high-order multiplicative interactions. However, from a learning perspective, it is clear that the CP layer has a natural inductive bias towards capturing high-order interactions. We are not enforcing any sparsity in the tensor parameterizing the polynomial, thus the number and magnitude of weights corresponding to high-order terms will dominate the result (intuitively, learning a low order polynomial would imply setting most of these weights to zero). In order to counterbalance this bias, we complement the CP layer with simple but efficient linear low-order interactions (reminiscent of the idea behind residual networks [21]) when using it in tGNN:

$$f(\mathbf{x}_1, \dots, \mathbf{x}_k) = \sigma' \left(\mathbf{M} \left(\sigma \left(\mathbf{W}_1^\top \begin{bmatrix} \mathbf{x}_1 \\ 1 \end{bmatrix} \odot \dots \odot \mathbf{W}_1^\top \begin{bmatrix} \mathbf{x}_k \\ 1 \end{bmatrix} \right) \right) \right) + \sigma''(\mathbf{W}_2^\top \mathbf{x}_1 + \dots + \mathbf{W}_2^\top \mathbf{x}_k) \quad (5)$$

where the first term corresponds to the CP layer and the second one to a standard sum pooling layer (with σ, σ' and σ'' being activation functions).

5 Related Work and Discussion

We now discuss relevant work on the parameterization of tensors on graph neural networks. In general, our work relates to three areas of deep learning: (1) aggregation functions, (2) universal approximator for set aggregation, (3) high-order pooling, and (4) tensor methods for deep learning.

GNN & Aggregation Scheme [26] successfully define convolutions on graph-structured data by averaging node information in a neighborhood. [48] prove the incomplete expressivity of mean aggregation to distinguish nodes, and further propose to use sum aggregation to differentiate nodes with similar properties. [13] further generalize this idea and show that mean aggregation can be a particular case of sum aggregation with a linear multiplier, and further propose an architecture with multiple aggregation channels to adaptively learn low-order information. Most GNNs use low-order aggregation schemes for learning node representations. To the best of our knowledge, tGNN is the first GNN architecture that adopts high-order multiplicative interactions in aggregation.

Universal Approximator & Permutation-invariant NN Universal approximators for set aggregation functions have been previously proposed and studied. [51] show that sum pooling is enough provided that it is combined with two universal approximators. [48] further discuss the limitations of non-injective set function. [25] propose a generalization of transformers to permutation-invariant sets. Most universal approximation results for GNN relies on combining simple aggregation functions (e.g. sum, mean) with universal approximators for the feature and output maps. In contrast, the CP layer achieves the same goal of being an universal approximator but using a different mean: explicit computation of multilinear polynomials (in an effective manner using the CP parameterization). While the approaches might be expressively similar, they may differ from a learning aspect, *i.e.*, how easy it is for these models to learn a function from data.

High-order Pooling [2] formulate the pooling problem as a multiset encoding problem with auxiliary information about the graph structure, and propose an attention-based pooling layer that captures the interaction between nodes according to their structural dependencies. [46] apply second-order statistic methods because the use of second-order statistics takes advantage of the Riemannian

geometry of the space of symmetric positive definite matrices. However, high-order in CP pooling refers to high-dimensional multiplicative feature products, which is different than previous literature.

Tensor Methods Tensor methods allow one to define meaningful geometries to build more expressive models. Authors in [52, 30] define geometries of tensor networks on complex or hypercomplex manifolds, their models encompass greater freedom in the choice of the product between the algebra elements. [7] develop a general framework for both probabilistic and neural models for tree-structured data with a tensor-based aggregation function. [6] leverages permutation-invariant CP-based aggregation function to capture high-order interactions in NLP tasks. Using multiplicative interactions as a powerful source of non-linearities in neural network models have been studied previously for convolutional [11, 10, 32] and recurrent networks [41, 44, 47]. The connection between such multiplicative interactions with tensor networks have been leveraged both from theoretical and practical perspectives. The CP layer can be seen as a graph generalization of the convolutional and recurrent arithmetic circuits considered in [10] and [31], respectively.

6 Experiments on Real-World Datasets

In this section, we evaluate Tensorized Graph Neural Net on real-world node- and graph-level datasets. We introduce experiment setup in 6.1, compare tGNN with the state-of-the-arts models in 6.2, and conduct ablation study on model performance and efficiency in 6.3. The hyperparameter and computing resources are attached in Appendix K. Dataset information can be found in Appendix J.

6.1 Experiment Setup

In this work, we conduct experiments on three citation networks (*Cora*, *Citeseer*, *Pubmed*) and three *OGB* datasets (*PRODUCTS*, *ARXIV*, *PROTEINS*) [23] for node-level tasks, one *OGB* dataset (*MolHIV*) [23] and three *benchmarking* datasets (*ZINC*, *CIFAR10*, *MNIST*) [14] for graph-level tasks.

Training Procedure For three citation networks (*Cora*, *Citeseer*, *Pubmed*), we run experiments 10 times on each dataset with 60%/20%/20% random splits used in [9], and report results in Tab. 1. For data splits of *OGB* node and graph datasets, we follow [23], run experiments 5 times on each dataset (due to training cost), and report results in Tab. 1, 2. For *benchmarking* datasets, we run experiments 5 times on each dataset with data split used in [14], and report results in Tab. 2. To avoid numerical instability and floating point exception in tGNN training, we sample 5 neighbors for each node. For graph datasets, we do not sample because the training is already in batch thus numerical instability can be avoided, and we apply the CP pooling at both node-level aggregation and graph-level readout.

Model Comparison tGNN has two hyperparameters, hidden unit and decomposition rank, we fix hidden unit and explore decomposition rank. For citation networks, we compare 2-layer GNNs with 32 hidden units. And for *OGB* and *benchmarking* datasets, we use 32 hidden units for tGNN, and the results for all other methods are reported from the leaderboards and corresponding references.

Particularly, tGNN and CP pooling are more effective and expressive than existing pooling techniques for GNNs on two citation networks, two *OGB* node datasets, and one *OGB* graph dataset in Tab. 1, 2.

6.2 Real-world Datasets

In this section, we present tGNN performance on node- and graph-level tasks. We compare tGNN with several classic baseline models under the same training setting. For three citation networks, we compare tGNN with several baselines including GCN [26], GAT [45], GraphSAGE [19], H₂GCN [54], GPRGNN [9], APPNP [27] and MixHop [1]; for three *OGB* node datasets, we compare tGNN with MLP, Node2vec [17], GCN [26], GraphSAGE [19] and DeeperGCN [33]. And for graph-level tasks, we compare tGNN with several baselines including MLP, GCN [26], GIN [48], DiffPool [50], GAT [45], MoNet [37], GatedGCN [4], PNA [13], PHMGNN [30] and DGN [3]. The model choice is because we propose a new pooling method and want to mainly compare tGNN with other poolings in standard GNN architectures. Current leading models on OGB leaderboards [23] adopt transformer, equivariant, fingerprint, C&S, or others, which are more complex than standard GNNs. We visualize the performance boost and comparisons with GNNs and pooling techniques in Tab. 1,2.

From Tab. 1, we can observe that tGNN outperforms all classic baselines on *Cora*, *Pubmed*, *PRODUCTS* and *ARXIV*, and have slight improvements on the other datasets but underperforms GCN on *Citeseer* and DeeperGCN on *PROTEINS*. On the citation networks, tGNN outperforms others on 2 out of 3 datasets. Moreover, on the *OGB* node datasets, even when tGNN is not ranked first, it is still very competitive (top 3 for all datasets). We believe it is reasonable and expected that tGNN does not outperform all methods on all datasets. But overall tGNN shows very competitive performance and

Table 1: Results of node-level tasks. **Left Table:** tGNN in comparison with GNN architectures on citation networks. **Right Table:** tGNN in comparison with GNN architectures on *OGB* datasets.

DATASET	<i>Cora</i>	<i>Citeseer</i>	<i>Pubmed</i>
MODEL	Acc	Acc	Acc
GCN	0.8778±0.0096	0.8139±0.0123	0.8890±0.0032
GAT	0.8686±0.0042	0.6720±0.0046	0.8328±0.0012
GraphSAGE	0.8658±0.0026	0.7624±0.0030	0.8658±0.0011
H ₂ GCN	0.8752±0.0061	0.7997±0.0069	0.8778±0.0028
GPRGNN	0.7951±0.0036	0.6763±0.0038	0.8507±0.0009
APPNP	0.7941±0.0038	0.6859±0.0030	0.8502±0.0009
MixHop	0.6565±0.1131	0.4952±0.1335	0.8704±0.0410
tGNN	0.8808±0.0131	0.8051±0.0192	0.9080±0.0018

DATASET	<i>PRODUCTS</i>	<i>ARXIV</i>	<i>PROTEINS</i>
MODEL	Acc	Acc	AUC
MLP	0.6106±0.0008	0.5550±0.0023	0.7204±0.0048
Node2vec	0.7249±0.0010	0.7007±0.0013	0.6881±0.0065
GCN	0.7564±0.0021	0.7174±0.0029	0.7251±0.0035
GraphSAGE	0.7850±0.0016	0.7149±0.0027	0.7768±0.0020
DeeperGCN	0.8098±0.0020	0.7192±0.0016	0.8580±0.0017
tGNN	0.8179±0.0054	0.7538±0.0015	0.8255±0.0049

deliver significant improvement on challenging graph benchmarks compared to popular commonly used pooling methods (with comparable computational cost).

Table 2: Results of tGNN on graph-level tasks in comparison with GNN architectures.

DATASET		<i>ZINC</i>	<i>CIFAR10</i>	<i>MNIST</i>	<i>MolHIV</i>
		No edge features MAE	No edge features Acc	No edge features Acc	No edge features AUC
Dwivedi et al. and Hu et al.	MLP	0.710±0.001	0.560±0.009	0.945±0.003	
	GCN	0.469±0.002	0.545±0.001	0.899±0.002	0.761±0.009
	GIN	0.408±0.008	0.533±0.037	0.939±0.013	0.756±0.014
	DiffPool	0.466±0.006	0.579±0.005	0.950±0.004	
	GAT	0.463±0.002	0.655±0.003	0.956±0.001	
	MoNet	0.407±0.007	0.534±0.004	0.904±0.005	
Corso et al.	GatedGCN	0.422±0.006	0.692±0.003	0.974±0.001	
	PNA	0.320±0.032	0.702±0.002	0.972±0.001	0.791±0.013
Le et al.	PHM-GNN				0.793±0.012
Beaini et al.	DGN	0.219±0.010	0.727±0.005		0.797±0.009
	Ours	tGNN	0.301±0.008	0.684±0.006	0.965±0.002

Table 3: Results of the tGNN ablation study on two node- and one graph-level tasks. tGNN in comparison with high-order CP pooling and low-order linear sum pooling.

DATASET	<i>Cora</i>	<i>Pubmed</i>	<i>ZINC</i>
MODEL	Acc	Acc	MAE
Non-Linear CP Pooling	0.8655±0.0375	0.8679±0.0103	0.407±0.025
Linear Sum Pooling	0.8623±0.0107	0.8531±0.0009	0.440±0.010
Non-Linear CP + Linear Sum	0.8780±0.0158	0.9018±0.0015	0.301±0.008

In Tab. 2, we present tGNN performance on graph property prediction tasks. tGNN achieves state-of-the-arts results on *MolHIV*, and have slight improvements on other three *Benchmarking* graph datasets. Overall tGNN achieves more effective and accurate results on 5 out of 10 datasets comparing with existing pooling techniques, which suggests that high-order CP pooling can leverage a GNN to generalize better node embeddings and graph representations.

6.3 Ablation and Efficiency Study

In the ablation study, we first investigate the effectiveness of having the high-order non-linear CP pooling and adding the linear low-order transformation in Tab. 3, then investigate the relations of the model performance, efficiency, and tensor decomposition rank in Fig. 4. Moreover, we compare tGNN with different GNN architectures and aggregation functions to show the efficiency in Tab. 5, 7 by showing the number of model parameters, computation time, and accuracy.

In Tab. 3, we test each component, high-order non-linear CP pooling, low-order linear sum pooling, and two pooling techniques combined, separately. We fix 2-layer GNNs with 32 hidden unit and 64 decomposition rank, and run experiments 10 times on *Cora* and *Pubmed* with 60%/20%/20% random splits used in [9], run *ZINC* 5 times with 10,000/1,000/1,000 graph split used in [14].

From the results, we can see that adding the linear low-order interactions helps put essential weights on them. Ablation results show that high-order CP pooling has the advantage over low-order linear pooling for generating expressive node and graph representations, moreover, tGNN is more expressive with the combination of high-order pooling and low-order aggregation. This illustrates the necessity of learning high-order components and low-order interactions simultaneously in tGNN.

Computational Aspect In Fig. 4, we compare model performance with computation costs. We fix a 2-layer tGNN with 32 hidden channels with 8,16,...,2048,4096 rank, and 2-layer baselines with 8,16,...,2048,4096 hidden dim. We run 10 times on each citation network with the same 60%/20%/20% random splits for train/validation/test and draw the relations of average test accuracy, rank/hidden dim, and computation costs. From the figure, we can see that the model performance can be improved with higher ranks (*i.e.*, Tensor \mathcal{T} is more accurately computed as the rank R gets larger), but training time is also increased, thus it is a trade-off between classification accuracy and

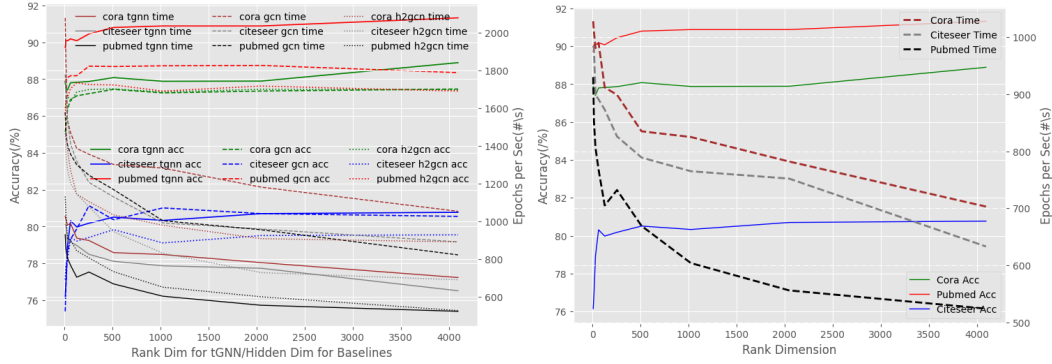


Figure 4: Results of node classification with increasing rank dimension on three citation datasets. **Left Figure:** Left axis shows accuracy, right axis shows #training epochs second, and horizontal axis indicates rank dim of tGNN or hidden dim of baselines. **Right Figure:** Left axis shows accuracy, right axis shows #training epochs second, and horizontal axis indicates rank dim of tGNN.

computation efficiency. And in comparison with baselines, tGNN still has marginal improvements with higher ranks while the baselines stop improving with larger hidden dimensions.

In Sec. 4.1, we theoretically discuss the time complexity of tGNN. In Appendix H, we experimentally assess model efficiency by comparing tGNN with GCN [26], GAT [45], GCN2 [8], and mean, max poolings on *Cora* on a CPU over 10 runtimes, and compare the number of model parameters, training epochs per second, and accuracy. The experiments show that tGNN is more competitive in terms of running time and better accuracy with a fixed number of parameters and the same time budget.

7 Conclusion and Future Work

In this paper, we theoretically develop a high-order permutation-invariant multilinear map for node aggregation and graph pooling via tensor parameterization. We show its powerful ability to compute any permutation-invariant multilinear polynomial including sum and mean pooling functions. Experiments demonstrate that tGNN is more effective and accurate on 5 out of 10 datasets, showcasing the relevance of tensor methods for high-order graph neural network models.

For future work, one interesting direction is to augment various GNN architectures with non-linear high-order CP layers. Most of the existing GNN models adopt low-order aggregation and pooling functions, it would be interesting to equip current state-of-the-art models with high-order pooling functions for a potential performance boost. Another interesting direction is to enhance tGNN with an adaptive channel mixing mechanism. In tGNN with high-order and low-order pooling functions, one node receives two channels of information combined in a linear way. The linear combination may not be sufficient to balance and extract high-order components and low-order components, so it would be interesting to design an adaptive channel mixing tGNN model for learning from different node-wise components.

Acknowledgements

This research was supported by the Canadian Institute for Advanced Research (CIFAR AI chair program) and the Natural Sciences and Engineering Research Council of Canada (Discovery program, RGPIN-2019-05949).

References

- [1] S. Abu-El-Haija, B. Perozzi, A. Kapoor, N. Alipourfard, K. Lerman, H. Harutyunyan, G. Ver Steeg, and A. Galstyan. Mixhop: Higher-order graph convolutional architectures via sparsified neighborhood mixing. In *international conference on machine learning*, pages 21–29. PMLR, 2019.
- [2] J. Baek, M. Kang, and S. J. Hwang. Accurate learning of graph representations with graph multiset pooling. *arXiv preprint arXiv:2102.11533*, 2021.
- [3] D. Beani, S. Passaro, V. Létourneau, W. Hamilton, G. Corso, and P. Liò. Directional graph networks. In *International Conference on Machine Learning*, pages 748–758. PMLR, 2021.
- [4] X. Bresson and T. Laurent. Residual gated graph convnets. *arXiv preprint arXiv:1711.07553*, 2017.
- [5] X. Cao and G. Rabusseau. Tensor regression networks with various low-rank tensor approximations. *arXiv preprint arXiv:1712.09520*, 2017.
- [6] D. Castellana and D. Bacciu. Learning from non-binary constituency trees via tensor decomposition. *arXiv preprint arXiv:2011.00860*, 2020.
- [7] D. Castellana and D. Bacciu. A tensor framework for learning in structured domains. *Neuro-computing*, 470:405–426, 2022.
- [8] M. Chen, Z. Wei, Z. Huang, B. Ding, and Y. Li. Simple and deep graph convolutional networks. In *International Conference on Machine Learning*, pages 1725–1735. PMLR, 2020.
- [9] E. Chien, J. Peng, P. Li, and O. Milenkovic. Adaptive universal generalized pagerank graph neural network. In *International Conference on Learning Representations*. <https://openreview.net/forum>, 2021.
- [10] N. Cohen, O. Sharir, and A. Shashua. Deep simnets. In *Proceedings of the IEEE Conference on Computer Vision and Pattern Recognition*, pages 4782–4791, 2016.
- [11] N. Cohen, O. Sharir, and A. Shashua. On the expressive power of deep learning: A tensor analysis. In *Conference on learning theory*, pages 698–728. PMLR, 2016.
- [12] P. Comon, G. Golub, L.-H. Lim, and B. Mourrain. Symmetric tensors and symmetric tensor rank. *SIAM Journal on Matrix Analysis and Applications*, 30(3):1254–1279, 2008.
- [13] G. Corso, L. Cavalleri, D. Beaini, P. Lio, and P. Velickovic. Principal neighbourhood aggregation for graph nets. *Advances in Neural Information Processing Systems*, 33:13260–13271, 2020.
- [14] V. P. Dwivedi, C. K. Joshi, T. Laurent, Y. Bengio, and X. Bresson. Benchmarking graph neural networks. *arXiv preprint arXiv:2003.00982*, 2020.
- [15] F. Errica, M. Podda, D. Bacciu, and A. Micheli. A fair comparison of graph neural networks for graph classification. *arXiv preprint arXiv:1912.09893*, 2019.
- [16] J. Gilmer, S. S. Schoenholz, P. F. Riley, O. Vinyals, and G. E. Dahl. Neural message passing for quantum chemistry. In *Proceedings of the 34th International Conference on Machine Learning-Volume 70*, pages 1263–1272. JMLR. org, 2017.
- [17] A. Grover and J. Leskovec. node2vec: Scalable feature learning for networks. In *Proceedings of the 22nd ACM SIGKDD international conference on Knowledge discovery and data mining*, pages 855–864. ACM, 2016.
- [18] W. L. Hamilton. Graph representation learning. *Synthesis Lectures on Artificial Intelligence and Machine Learning*, 14(3):1–159, 2020.
- [19] W. L. Hamilton, R. Ying, and J. Leskovec. Inductive representation learning on large graphs. *arXiv*, abs/1706.02216, 2017.
- [20] W. L. Hamilton, R. Ying, and J. Leskovec. Representation learning on graphs: Methods and applications. *arXiv preprint arXiv:1709.05584*, 2017.
- [21] K. He, X. Zhang, S. Ren, and J. Sun. Deep residual learning for image recognition. In *Proceedings of the IEEE conference on computer vision and pattern recognition*, pages 770–778, 2016.
- [22] F. L. Hitchcock. The expression of a tensor or a polyadic as a sum of products. *Journal of Mathematics and Physics*, 6(1-4):164–189, 1927.

- [23] W. Hu, M. Fey, M. Zitnik, Y. Dong, H. Ren, B. Liu, M. Catasta, and J. Leskovec. Open graph benchmark: Datasets for machine learning on graphs. *arXiv preprint arXiv:2005.00687*, 2020.
- [24] H. A. Kiers. Towards a standardized notation and terminology in multiway analysis. *Journal of Chemometrics: A Journal of the Chemometrics Society*, 14(3):105–122, 2000.
- [25] J. Kim, S. Oh, and S. Hong. Transformers generalize deepsets and can be extended to graphs & hypergraphs. *Advances in Neural Information Processing Systems*, 34, 2021.
- [26] T. N. Kipf and M. Welling. Semi-supervised classification with graph convolutional networks. *arXiv*, abs/1609.02907, 2016.
- [27] J. Klicpera, A. Bojchevski, and S. Günnemann. Predict then propagate: Graph neural networks meet personalized pagerank. *arXiv preprint arXiv:1810.05997*, 2018.
- [28] T. G. Kolda. Numerical optimization for symmetric tensor decomposition. *Mathematical Programming*, 151(1):225–248, 2015.
- [29] T. G. Kolda and B. W. Bader. Tensor decompositions and applications. *SIAM review*, 51(3):455–500, 2009.
- [30] T. Le, M. Bertolini, F. Noé, and D.-A. Clevert. Parameterized hypercomplex graph neural networks for graph classification. *arXiv preprint arXiv:2103.16584*, 2021.
- [31] Y. Levine, O. Sharir, and A. Shashua. Benefits of depth for long-term memory of recurrent networks. 2018.
- [32] Y. Levine, D. Yakira, N. Cohen, and A. Shashua. Deep learning and quantum entanglement: Fundamental connections with implications to network design. In *International Conference on Learning Representations*, 2018.
- [33] G. Li, C. Xiong, A. Thabet, and B. Ghanem. Deepergcn: All you need to train deeper gens. *arXiv preprint arXiv:2006.07739*, 2020.
- [34] S. Luan, C. Hua, Q. Lu, J. Zhu, M. Zhao, S. Zhang, X.-W. Chang, and D. Precup. Is heterophily a real nightmare for graph neural networks to do node classification? *arXiv preprint arXiv:2109.05641*, 2021.
- [35] S. Luan, C. Hua, Q. Lu, J. Zhu, M. Zhao, S. Zhang, X.-W. Chang, and D. Precup. Revisiting heterophily for graph neural networks. *arXiv preprint arXiv:2210.07606*, 2022.
- [36] S. Luan, M. Zhao, C. Hua, X.-W. Chang, and D. Precup. Complete the missing half: Augmenting aggregation filtering with diversification for graph convolutional networks. *arXiv preprint arXiv:2008.08844*, 2020.
- [37] F. Monti, D. Boscaini, J. Masci, E. Rodola, J. Svoboda, and M. M. Bronstein. Geometric deep learning on graphs and manifolds using mixture model cnns. In *Proceedings of the IEEE conference on computer vision and pattern recognition*, pages 5115–5124, 2017.
- [38] A. Novikov, M. Trofimov, and I. Oseledets. Exponential machines. *arXiv preprint arXiv:1605.03795*, 2016.
- [39] Y. Peng, A. Ganesh, J. Wright, W. Xu, and Y. Ma. Rasl: Robust alignment by sparse and low-rank decomposition for linearly correlated images. *IEEE transactions on pattern analysis and machine intelligence*, 34(11):2233–2246, 2012.
- [40] G. Rabusseau and H. Kadri. Low-rank regression with tensor responses. *Advances in Neural Information Processing Systems*, 29, 2016.
- [41] O. Sharir and A. Shashua. On the expressive power of overlapping architectures of deep learning. *arXiv preprint arXiv:1703.02065*, 2017.
- [42] C. Shi, M. Xu, Z. Zhu, W. Zhang, M. Zhang, and J. Tang. Graphaf: a flow-based autoregressive model for molecular graph generation. *arXiv preprint arXiv:2001.09382*, 2020.
- [43] E. M. Stoudenmire and D. J. Schwab. Supervised learning with quantum-inspired tensor networks. arxiv 2016. *arXiv preprint arXiv:1605.05775*.
- [44] I. Sutskever, J. Martens, and G. E. Hinton. Generating text with recurrent neural networks. In *ICML*, 2011.
- [45] P. Velickovic, G. Cucurull, A. Casanova, A. Romero, P. Lio, and Y. Bengio. Graph attention networks. *arXiv*, abs/1710.10903, 2017.

- [46] Z. Wang and S. Ji. Second-order pooling for graph neural networks. *IEEE Transactions on Pattern Analysis and Machine Intelligence*, 2020.
- [47] Y. Wu, S. Zhang, Y. Zhang, Y. Bengio, and R. R. Salakhutdinov. On multiplicative integration with recurrent neural networks. *Advances in neural information processing systems*, 29, 2016.
- [48] K. Xu, W. Hu, J. Leskovec, and S. Jegelka. How powerful are graph neural networks? *arXiv preprint arXiv:1810.00826*, 2018.
- [49] R. Ying, R. He, K. Chen, P. Eksombatchai, W. L. Hamilton, and J. Leskovec. Graph convolutional neural networks for web-scale recommender systems. In *Proceedings of the 24th ACM SIGKDD International Conference on Knowledge Discovery & Data Mining*, pages 974–983, 2018.
- [50] R. Ying, J. You, C. Morris, X. Ren, W. L. Hamilton, and J. Leskovec. Hierarchical graph representation learning with differentiable pooling. *arXiv preprint arXiv:1806.08804*, 2018.
- [51] M. Zaheer, S. Kottur, S. Ravanbakhsh, B. Póczos, R. R. Salakhutdinov, and A. J. Smola. Deep sets. *Advances in neural information processing systems*, 30, 2017.
- [52] S. Zhang, Y. Tay, L. Yao, and Q. Liu. Quaternion knowledge graph embeddings. *arXiv preprint arXiv:1904.10281*, 2019.
- [53] X. Zhang, Z.-H. Huang, and L. Qi. Comon’s conjecture, rank decomposition, and symmetric rank decomposition of symmetric tensors. *SIAM Journal on Matrix Analysis and Applications*, 37(4):1719–1728, 2016.
- [54] J. Zhu, Y. Yan, L. Zhao, M. Heimann, L. Akoglu, and D. Koutra. Beyond homophily in graph neural networks: Current limitations and effective designs. *Advances in Neural Information Processing Systems*, 33, 2020.
- [55] Z. Zhu, Z. Zhang, L.-P. Xhonneux, and J. Tang. Neural bellman-ford networks: A general graph neural network framework for link prediction. *arXiv preprint arXiv:2106.06935*, 2021.

A Proof of Theorem 1

In order to prove this theorem, we first need the following lemma showing the existence of partially symmetric CP decompositions.

Lemma 1. *Any partially symmetric tensor admits a partially symmetric CP decomposition.*

Proof. We show the results for 3-rd order tensors that are partially symmetric w.r.t. their two first modes. The proof can be straightforwardly extended to tensors of arbitrary order that are partially symmetric w.r.t. any subset of modes.

Let $\mathcal{T} \in \mathbb{R}^{m \times m \times n}$ be partially symmetric w.r.t. modes 1 and 2. We have that $\mathcal{T}_{::,i}$ is a symmetric tensor for each $i \in [n]$. By Lemma 4.2 in [12], each tensor $\mathcal{T}_{::,i}$ admits a symmetric CP decomposition:

$$\mathcal{T}_{::,i} = \llbracket \mathbf{A}^{(i)}, \mathbf{A}^{(i)} \rrbracket, \quad i \in [n]$$

where $\mathbf{A}^{(i)} \in \mathbb{R}^{m \times R_i}$ and R_i is the symmetric CP rank of $\mathcal{T}_{::,i}$.

By defining $R = \sum_{i=1}^n R_i$ and $\mathbf{A} = [\mathbf{A}^{(1)} \ \mathbf{A}^{(2)} \ \dots \ \mathbf{A}^{(n)}] \in \mathbb{R}^{m \times R}$, one can easily check that \mathcal{T} admits the partially symmetric CP decomposition $\mathcal{T} = \llbracket \mathbf{A}, \mathbf{A}, \mathbf{\Delta} \rrbracket$ where $\mathbf{\Delta} \in \mathbb{R}^{m \times R}$ is defined by

$$\Delta_{i,r} = \begin{cases} 1 & \text{if } R_1 + \dots + R_{i-1} < r \leq R_1 + \dots + R_i \\ 0 & \text{otherwise.} \end{cases}$$

□

We can now prove Theorem 1.

Theorem. *The function computed by a CP layer (Eq. equation 1) is permutation-invariant. In addition, any permutation-invariant multilinear polynomial $f : (\mathbb{R}^F)^k \rightarrow \mathbb{R}^d$ can be computed by a CP layer (with linear activation function).*

Proof. The fact that the function computed by a CP layer is permutation-invariant directly follows from the definition of the CP layer and the fact that the Hadamard product is commutative.

We now show the second part of the theorem. Let $f : (\mathbb{R}^F)^k \rightarrow \mathbb{R}^d$ be a permutation-invariant multilinear polynomial map. Then, there exists permutation-invariant univariate multilinear polynomials g_{i,j_1,\dots,j_k} for $j_1, \dots, j_k \in [F]$ and $i \in [d]$ such that

$$f(\mathbf{x}_1, \dots, \mathbf{x}_k)_i = \sum_{j_1=1}^d \dots \sum_{j_k=1}^d g_{i,j_1,\dots,j_k}((\mathbf{x}_1)_{j_1}, \dots, (\mathbf{x}_k)_{j_k}).$$

Moreover, by definition, each such polynomial satisfies

$$g_{i,j_1,\dots,j_k}(a_1, a_2, \dots, a_k) = \sum_{i_1=0}^1 \dots \sum_{i_k=0}^1 \tau_{i_1,\dots,i_k}^{(i,j_1,\dots,j_k)} a_1^{i_1} a_2^{i_2} \dots a_k^{i_k}$$

for some scalars $\tau_{i_1,\dots,i_k}^{(i,j_1,\dots,j_k)}$. Putting those two expressions together, we get

$$f(\mathbf{x}_1, \dots, \mathbf{x}_k)_i = \sum_{j_1=1}^d \dots \sum_{j_k=1}^d \sum_{i_1=0}^1 \dots \sum_{i_k=0}^1 \tau_{i_1,\dots,i_k}^{(i,j_1,\dots,j_k)} (\mathbf{x}_1)_{j_1}^{i_1} \dots (\mathbf{x}_k)_{j_k}^{i_k}.$$

We can then group together the coefficients $\tau_{i_1,\dots,i_k}^{(i,j_1,\dots,j_k)}$ corresponding to the same monomials $(\mathbf{x}_1)_{j_1}^{i_1} \dots (\mathbf{x}_k)_{j_k}^{i_k}$. E.g., the coefficients $\tau_{1,0,\dots,0}^{(i,j_1,\dots,j_k)}$ all correspond to the same monomial $(\mathbf{x}_1)_{j_1}$ for any values of j_2, j_3, \dots, j_k . Similarly, all the coefficients $\tau_{0,1,\dots,1}^{(i,j_1,\dots,j_k)}$ all correspond to the same monomial $(\mathbf{x}_2)_{j_2} \dots (\mathbf{x}_k)_{j_k}$ for any values of j_1 . By grouping and summing together these coefficients into a tensor $\mathcal{T} \in \mathbb{R}^{(F+1) \times \dots \times (F+1) \times d}$, where $\mathcal{T}_{j_1,\dots,j_k,i}$ is equal to the sum

$\sum_{j_\ell \in [F]: j_\ell = F+1 \wedge i_\ell = 0} \tau_{i_1,\dots,i_k}^{(i,j_1,\dots,j_k)}$, we obtain

$$f(\mathbf{x}_1, \dots, \mathbf{x}_k)_i = \sum_{j_1=1}^{F+1} \sum_{j_2=1}^{F+1} \dots \sum_{j_k=1}^{F+1} \mathcal{T}_{j_1,j_2,\dots,j_k,i} \begin{pmatrix} \mathbf{x}_1 \\ 1 \end{pmatrix}_{j_1} \begin{pmatrix} \mathbf{x}_2 \\ 1 \end{pmatrix}_{j_2} \dots \begin{pmatrix} \mathbf{x}_k \\ 1 \end{pmatrix}_{j_k}.$$

Since f is permutation-invariant, the tensor \mathcal{T} is partially symmetric w.r.t. its first k modes. Thus, by Lemma 1, there exist matrices $\mathbf{A} \in \mathbb{R}^{R \times F}$ and $\mathbf{B} \in \mathbb{R}^{d \times R}$ such that

$$\begin{aligned} f(\mathbf{x}_1, \dots, \mathbf{x}_k) &= \mathcal{T} \times_1 \begin{bmatrix} \mathbf{x}_1 \\ 1 \end{bmatrix} \times_2 \cdots \times_k \begin{bmatrix} \mathbf{x}_k \\ 1 \end{bmatrix} \\ &= \llbracket \mathbf{A}, \dots, \mathbf{A}, \mathbf{B} \rrbracket \times_1 \begin{bmatrix} \mathbf{x}_1 \\ 1 \end{bmatrix} \times_2 \cdots \times_k \begin{bmatrix} \mathbf{x}_k \\ 1 \end{bmatrix} \\ &= \mathbf{B} \sigma \left(\mathbf{A}^\top \begin{bmatrix} \mathbf{x}_1 \\ 1 \end{bmatrix} \odot \cdots \odot \mathbf{A}^\top \begin{bmatrix} \mathbf{x}_k \\ 1 \end{bmatrix} \right) \end{aligned}$$

with σ being the identity function, which concludes the proof. \square

B Proof of Theorem 2

Theorem. A CP layer of rank $F \cdot k$ can compute the sum and mean aggregation functions for k vectors in \mathbb{R}^F .

Consequently, for any $k \geq 1$ and any GNN \mathcal{N} using mean or sum pooling with feature and embedding dimensions bounded by F , there exists a GNN with CP layers of rank $F \cdot k$ computing the same function as \mathcal{N} over all graphs of uniform degree k .

Proof. We will show that the function $f : (\mathbb{R}^F)^k \rightarrow \mathbb{R}^d$ defined by

$$f(\mathbf{x}_1, \dots, \mathbf{x}_k) = \sum_{i=1}^k \alpha \mathbf{x}_i$$

where $\alpha \in \mathbb{R}$, can be computed by a CP layer of rank Fk , which will show the first part of the theorem. The second part of the theorem directly follows by letting $\alpha = 1$ for the sum aggregation and $\alpha = 1/k$ for the mean aggregation.

Let $\tilde{\mathbf{e}}_1, \dots, \tilde{\mathbf{e}}_{F+1}$ be the canonical basis of \mathbb{R}^{F+1} , and let $\mathbf{e}_1, \dots, \mathbf{e}_F$ be the canonical basis of \mathbb{R}^F . We define the tensor $\mathcal{T} \in \mathbb{R}^{(F+1) \times \cdots \times (F+1) \times d}$ by

$$\mathcal{T} = \sum_{j=1}^d \sum_{\ell=1}^k \alpha \underbrace{\tilde{\mathbf{e}}_{F+1} \circ \cdots \circ \tilde{\mathbf{e}}_{F+1}}_{\ell-1 \text{ times}} \circ \tilde{\mathbf{e}}_j \circ \underbrace{\tilde{\mathbf{e}}_{F+1} \circ \cdots \circ \tilde{\mathbf{e}}_{F+1}}_{k-\ell \text{ times}} \circ \mathbf{e}_j$$

where \circ denotes the outer (or tensor) product between vectors. We start by showing that contracting k vectors in homogeneous coordinates along the first k modes of \mathcal{T} results in the sum of those vectors weighted by α . For any vectors $\mathbf{x}_1, \dots, \mathbf{x}_k \in \mathbb{R}^F$, we have

$$\begin{aligned} \mathcal{T} \times_1 \begin{bmatrix} \mathbf{x}_1 \\ 1 \end{bmatrix} \times_2 \cdots \times_k \begin{bmatrix} \mathbf{x}_k \\ 1 \end{bmatrix} &= \left(\sum_{j=1}^d \sum_{\ell=1}^k \alpha \underbrace{\tilde{\mathbf{e}}_{F+1} \circ \cdots \circ \tilde{\mathbf{e}}_{F+1}}_{\ell-1 \text{ times}} \circ \tilde{\mathbf{e}}_j \circ \underbrace{\tilde{\mathbf{e}}_{F+1} \circ \cdots \circ \tilde{\mathbf{e}}_{F+1}}_{k-\ell \text{ times}} \circ \mathbf{e}_j \right) \times_1 \begin{bmatrix} \mathbf{x}_1 \\ 1 \end{bmatrix} \times_2 \cdots \times_k \begin{bmatrix} \mathbf{x}_k \\ 1 \end{bmatrix} \\ &= \sum_{j=1}^d \sum_{\ell=1}^k \alpha \langle \tilde{\mathbf{e}}_{F+1}, \begin{bmatrix} \mathbf{x}_1 \\ 1 \end{bmatrix} \rangle \cdots \langle \tilde{\mathbf{e}}_{F+1}, \begin{bmatrix} \mathbf{x}_{\ell-1} \\ 1 \end{bmatrix} \rangle \langle \tilde{\mathbf{e}}_j, \begin{bmatrix} \mathbf{x}_\ell \\ 1 \end{bmatrix} \rangle \langle \tilde{\mathbf{e}}_{F+1}, \begin{bmatrix} \mathbf{x}_{\ell+1} \\ 1 \end{bmatrix} \rangle \cdots \langle \tilde{\mathbf{e}}_{F+1}, \begin{bmatrix} \mathbf{x}_k \\ 1 \end{bmatrix} \rangle \mathbf{e}_j \\ &= \sum_{j=1}^d \sum_{\ell=1}^k (\alpha \cdot 1 \cdots 1 \cdot \langle \mathbf{x}_\ell, \mathbf{e}_j \rangle \cdot 1 \cdots 1) \mathbf{e}_j \\ &= \sum_{j=1}^d \left\langle \sum_{\ell=1}^k \alpha \mathbf{x}_\ell, \mathbf{e}_j \right\rangle \mathbf{e}_j \\ &= \sum_{\ell=1}^k \alpha \mathbf{x}_\ell = f(\mathbf{x}_1, \dots, \mathbf{x}_k). \end{aligned}$$

To show that f can be computed by a CP layer of rank Fk , it thus remains to show that \mathcal{T} admits a partially symmetric CP decomposition of rank Fk . This follows from Corollary 4.3 in [53], which

states that any k th order tensor \mathcal{A} of CP rank less than k has symmetric CP rank bounded by k . Indeed, consider the tensors

$$\mathcal{A}^{(j)} = \sum_{\ell=1}^k \alpha \underbrace{\tilde{\mathbf{e}}_{F+1} \circ \cdots \circ \tilde{\mathbf{e}}_{F+1}}_{\ell-1 \text{ times}} \circ \tilde{\mathbf{e}}_j \circ \underbrace{\tilde{\mathbf{e}}_{F+1} \circ \cdots \circ \tilde{\mathbf{e}}_{F+1}}_{k-\ell \text{ times}}$$

for $j \in [d]$. They are all k -th order tensor of CP rank bounded by k . Thus, by Corollary 4.3 in [53], they all admit a symmetric CP decomposition of rank at most k , from which it directly follows that the tensor $\mathcal{T} = \sum_{j=1}^F \mathcal{A}^{(j)} \circ \mathbf{e}_j$ admits a partially symmetric CP decomposition of rank at most Fk . \square

C Proof of Theorem 3

Theorem. *With probability one, any function $f_{CP} : (\mathbb{R}^F)^k \rightarrow \mathbb{R}^d$ computed by a CP layer (of any rank) whose parameters are drawn randomly (from a continuous distribution) cannot be computed by a function of the form*

$$g_{sum} : \mathbf{x}_1, \dots, \mathbf{x}_k \mapsto \sigma' \left(\mathbf{M} \left(\sigma \left(\sum_{i=1}^k \mathbf{W}^\top \mathbf{x}_i \right) \right) \right)$$

where $\mathbf{M} \in \mathbb{R}^{d \times R}$, $\mathbf{W} \in \mathbb{R}^{F \times R}$ and σ, σ' are component-wise activation function.

Proof. Let $f_{CP} : (\mathbb{R}^F)^k \rightarrow \mathbb{R}^d$ be the function computed by a random CP layer. I.e.,

$$f_{CP}(\mathbf{x}_1, \dots, \mathbf{x}_k) = \mathbf{A} \left(\left(\mathbf{B}^\top \begin{bmatrix} \mathbf{x}_1 \\ 1 \end{bmatrix} \right) \odot \cdots \odot \left(\mathbf{B}^\top \begin{bmatrix} \mathbf{x}_k \\ 1 \end{bmatrix} \right) \right)$$

where the entries of the matrices $\mathbf{B} \in \mathbb{R}^{(N+1) \times R}$ and $\mathbf{A} \in \mathbb{R}^{M \times R}$ are identically and independently drawn from a distribution which is continuous w.r.t. the Lebesgue measure. It is well know that since the entries of the two parameter matrices are drawn from a continuous distribution, all the entries of \mathbf{A} and \mathbf{B} are non-zero and distinct with probability one. It follows that all the entries of the vector $f_{CP}(\mathbf{x}_1, \dots, \mathbf{x}_k)$ are k -th order multilinear polynomials of the entries of the input vectors $\mathbf{x}_1, \dots, \mathbf{x}_k$, which, with probability one, have non trivial high-order interactions that cannot be computed by a linear map. In particular, with probability one, the map f_{CP} cannot be computed by any map of the form $g_{sum} : \mathbf{x}_1, \dots, \mathbf{x}_k \mapsto \sigma' \left(\mathbf{M} \left(\sigma \left(\sum_{i=1}^k \mathbf{W}^\top \mathbf{x}_i \right) \right) \right)$ since the sum pooling aggregates the inputs in a way that prevents modeling independent higher order multiplicative interactions, despite the non-linear activation functions. \square

D Rank and Performance

Generally speaking, the low-rank decomposition methods will sacrifice some expressivity for some computation costs, so as we increase the rank, we will re-gain some expressivity but lose some computation costs. As talked about in our paper, it is a trade-off between expressivity (model performance) and computation costs. This idea can be found in previous works [39, 40, 5] where they test on computer vision datasets (with visualization of recovering images from noises, a high-rank model can always better recover an image than a low-rank model does).

In this work, we use the low-rank decomposition technique which can potentially reduce the number of learnable parameters by a lower number of ranks. The low-rank method saves the computation costs but the use of low-rank decomposition for learnable parameters will sacrifice some expressivity in computation. If we increase the rank, the learnable parameters can be principally recovered, in this case, we no longer sacrifice its expressivity but computation costs (as the Figures shown in the ablation study).

In computer vision, low-rank decomposition methods were introduced to replace a fully-connected layer. And in their papers [39, 40, 5] (in both theory and experiments), they show that a model is better with higher ranks because higher ranks can lead to higher expressivity than low ranks do. They conclude and show that the model performance is positively correlated to the tensor decomposition

rank. In [39, 40, 5], they experimentally show that higher ranks can result in lower test errors as the model becomes more expressive (plotting a curve of decomposition rank or model parameter vs. error). Moreover, in [39, 40], they visualize the relationship between the model performance and model rank. They aim to recover the original pictures from noises with different tensor ranks (from low to high), and the recovered pictures are more clear with high ranks than with low ranks. To conclude our findings in the ablation study and previous works on low-rank decomposition, high-rank models can usually have better performance and stronger expressivity than low-rank models, and higher ranks can usually lead to better performance (in terms of high accuracy or low error) than low ranks do.

E Low and High Terms

The reason we introduce the inductive bias is that we want to balance the importance of low- and high-order terms. We design an experiment to show which interactions play the main role. We have two learnable attention weights a_{low}, a_{high} , one before high-order terms and the other one before low-order terms, node representation $H = a_{high}H_{high} + a_{low}H_{low}$ with $a_{low} + a_{high} = 1$. If high-order interactions dominate a_{high} will be larger, else if low-order interactions dominate a_{low} will be larger. At the early model learning stage, a_{high} is a lot higher (~ 0.9) than a_{low} (~ 0.1), which show high-order terms dominate at the beginning, and a_{high}, a_{low} will converge to a similar value (~ 0.5) as the model improves, which show that low- and high-order terms have the similar importance.

F GCN Performance

We do see in our Tables, GCN can beat popular baselines. It is not really weird, if you can do a full hyperparameter search (either GCN built on PyG or Torch), you'll find out that GCN can outperform the most popular GNN architectures (after GCN gets proposed). And the papers [36, 34] find out the same experimental phenomenon. The question, that GCN can outperform a lot GNNs on many (heterophilic or homophilic) datasets after thorough hyperparameter tuning, was discussed in the community before but never raised attention.

G Additional Graph Classification

[2] formulate the graph pooling problem as a multiset encoding problem with auxiliary information about the graph structure, and propose an attention-based pooling layer that captures the interaction between nodes according to their structural dependencies. [46] apply second-order statistic methods because the use of second-order statistics takes advantage of the Riemannian geometry of the space of symmetric positive definite matrices. Their formulation adapts the bilinear pooling, and the bilinear mapping is capable of capturing second-order statistics and topology information.

We test and compare tGNN with [2, 46] following the setting of [15].

Table 4: Study of Efficiency vs. Performance on Cora. tGNN in comparison with GNN architectures with more sampled neighbor nodes.

	MUTAG	PROTEINS	IMDB-B	IMDB-M	COLLAB
GIN	81.4 ± 1.5	71.5 ± 1.7	72.8 ± 0.9	48.1 ± 1.4	78.2 ± 0.6
GMT	83.6 ± 2.3	74.7 ± 1.8	73.5 ± 0.6	49.8 ± 1.1	81.1 ± 1.6
SOPPool	82.7 ± 1.6	72.5 ± 2.4	73.3 ± 1.9	48.7 ± 3.0	79.0 ± 1.9
tGNN	84.4 ± 1.9	75.3 ± 2.0	73.8 ± 0.9	49.1 ± 1.5	82.1 ± 2.7

The table records graph classification results on test sets for 5 graph-level tasks under the setting of [15]. We can see that our model makes improvements on 4 out of 5 datasets (big improvements on MUTAG, PROTEINS, and COLLAB, and small improvements on IMDB-B).

H Efficiency Study

We study efficiency by comparing tGNN with models on Cora on a CPU over 10 runtimes, and compare the number of model parameters, number of training epochs per second, and accuracy.

Sampling means we sample '3' neighbors for each node or we use 'Full' neighborhood. Notice that the average node degree of Cora is 3.9, which means if a node has a number of neighbors less than 10, some of its neighbor nodes will get resampled until it hits 10.

Table 5: Study of Efficiency vs. Performance on Cora. tGNN in comparison with GNN architectures.

	Dropout	LR	Weight Decay	Hidden	Rank	Head	Sampling	#Params	Time(s)	Epoch	Epoch/s	Acc	Std
tGNN	0	0.005	5.00E-05	32	8	-	3	58128	290.9774	1389	4.7736	85.55	1.33
tGNN	0	0.005	5.00E-05	32	32	-	3	94272	790.0373	1321	1.6721	86.25	0.58
tGNN	0	0.005	5.00E-05	32	64	-	3	142464	383.2255	1343	3.5045	86.06	1.08
tGNN	0	0.005	5.00E-05	32	128	-	3	238848	999.1514	1247	1.2481	86.76	1.19
tGNN	0	0.005	5.00E-05	32	256	-	3	431616	1193.7131	1272	1.0656	86.97	1.24
tGNN	0	0.005	5.00E-05	32	512	-	3	817152	1621.9083	1332	0.8213	87.33	1.83
tGNN	0	0.005	5.00E-05	32	1024	-	3	1588224	2377.5139	1265	0.5321	87.62	1.63
GCN	0	0.005	5.00E-05	32	-	-	3	46080	212.3576	1509	7.1059	84.29	1.02
GCN	0	0.005	5.00E-05	32	-	-	Full	46080	205.0601	1276	6.2226	85.24	1.69
GCN	0	0.005	5.00E-05	64	-	-	3	92160	316.6461	1240	3.916	85.12	2.11
GCN	0	0.005	5.00E-05	64	-	-	Full	92160	318.3962	1161	3.6464	85.59	2.03
GAT	0	0.005	5.00E-05	32	-	1	3	92238	605.3269	1998	3.3007	83.66	1.54
GAT	0	0.005	5.00E-05	32	-	1	Full	92238	548.7319	1638	2.9851	84.79	2.26
GAT	0	0.005	5.00E-05	32	-	8	3	762992	1491.5643	1594	1.069	86.26	1.35
GAT	0	0.005	5.00E-05	32	-	8	Full	762992	1524.4348	1276	0.837	87.07	1.64
GAT	0	0.005	5.00E-05	64	-	1	3	184462	626.4011	1740	2.7778	84.15	1.29
GAT	0	0.005	5.00E-05	64	-	1	Full	184462	682.7776	1465	2.1456	86.07	2.55
GAT	0	0.005	5.00E-05	64	-	8	3	1525872	2164.689	1348	0.6227	85.32	1.31
GAT	0	0.005	5.00E-05	64	-	8	Full	1525872	2143.036	1105	0.5156	87.01	0.96
GCN2	0	0.005	5.00E-05	32	-	-	3	48128	256.9575	1708	6.647	83.17	1.5
GCN2	0	0.005	5.00E-05	32	-	-	Full	48128	210.7702	1302	6.1773	84.38	2.03
GCN2	0	0.005	5.00E-05	64	-	-	3	100352	353.0055	1581	4.4787	84.7	1.13
GCN2	0	0.005	5.00E-05	64	-	-	Full	100352	307.7913	1219	3.9605	84.79	1.64
GCN2	0	0.005	5.00E-05	Input Dim	-	-	3	4117009	3013.6082	1051	0.3488	86.72	1.82
GCN2	0	0.005	5.00E-05	Input Dim	-	-	Full	4117009	3091.4392	1013	0.3277	87.54	1.66

From Table 6, we can see that the model performance is not heavily affected by the number of sampled neighbor nodes because the average node degree is not that high on the majority of network datasets, and '3' or '5' would be sufficient.

Table 6: Study of Efficiency vs. Performance on Cora. tGNN in comparison with GNN architectures with more sampled neighbor nodes (3 vs. 10).

	Dropout	LR	Weight Decay	Hidden	Rank	Head	Sampling	#Params	Time(s)	Epoch	Epoch/s	Acc	Std
tGNN	0	0.005	5E-5	32	8	-	3	58128	290.9774	1389	4.7736	85.55	1.33
tGNN	0	0.005	5E-5	32	32	-	3	94272	383.2255	1321	3.5045	86.25	0.58
tGNN	0	0.005	5E-5	32	64	-	3	142464	790.0373	1343	1.6721	86.06	1.08
tGNN	0	0.005	5E-5	32	128	-	3	238848	999.1514	1247	1.2481	86.76	1.19
tGNN	0	0.005	5E-5	32	256	-	3	431616	1193.7131	1272	1.0656	86.97	1.24
tGNN	0	0.005	5E-5	32	512	-	3	817152	1621.9083	1332	0.8213	87.33	1.83
tGNN	0	0.005	5E-5	32	1024	-	3	1588224	2377.5139	1265	0.5321	87.62	1.63
tGNN	0	0.005	5E-5	32	8	-	10	58128	330.8677	1379	4.1678	85.40	1.55
tGNN	0	0.005	5E-5	32	32	-	10	94272	520.9030	1331	2.5552	86.35	1.37
tGNN	0	0.005	5E-5	32	64	-	10	142464	810.5341	1365	1.6841	86.83	1.28
tGNN	0	0.005	5E-5	32	128	-	10	238848	1170.4560	1381	1.1799	86.77	0.94
tGNN	0	0.005	5E-5	32	256	-	10	431616	1890.5941	1357	0.7178	87.42	1.01
tGNN	0	0.005	5E-5	32	512	-	10	817152	2048.7935	1326	0.6472	87.22	1.57
tGNN	0	0.005	5E-5	32	1024	-	10	1588224	2843.5611	1339	0.4709	87.87	1.42
GCN	0	0.005	5E-5	32	-	-	3	46080	212.3576	1509	7.1059	84.29	1.02
GCN	0	0.005	5E-5	32	-	-	10	46080	250.4735	1290	5.1502	85.33	1.35
GCN	0	0.005	5E-5	32	-	-	Full	46080	205.0601	1276	6.2226	85.24	1.69
GCN	0	0.005	5E-5	64	-	-	3	92160	316.6461	1240	3.916	85.12	2.11
GCN	0	0.005	5E-5	64	-	-	10	92160	398.3892	1049	2.6331	85.50	1.78
GCN	0	0.005	5E-5	64	-	-	Full	92160	318.3962	1161	3.6464	85.59	2.03
GAT	0	0.005	5E-5	32	-	1	3	92238	605.3269	1998	3.3007	83.66	1.54
GAT	0	0.005	5E-5	32	-	1	10	92238	550.6742	1438	2.5968	84.66	1.57
GAT	0	0.005	5E-5	32	-	1	Full	92238	548.7319	1638	2.9851	84.79	2.26
GAT	0	0.005	5E-5	32	-	8	3	762992	1491.5643	1594	1.069	86.26	1.35
GAT	0	0.005	5E-5	32	-	8	10	762992	1678.9020	1285	0.7654	87.08	1.45
GAT	0	0.005	5E-5	32	-	8	Full	762992	1524.4348	1276	0.837	87.07	1.64
GAT	0	0.005	5E-5	64	-	1	3	184462	626.4011	1740	2.7778	84.15	1.29
GAT	0	0.005	5E-5	64	-	1	10	184462	740.5192	1311	1.7704	86.01	1.65
GAT	0	0.005	5E-5	64	-	1	Full	184462	682.7776	1465	2.1456	86.07	2.55
GAT	0	0.005	5E-5	64	-	8	3	1525872	2164.689	1348	0.6227	85.32	1.31
GAT	0	0.005	5E-5	64	-	8	10	1525872	2580.3489	1205	0.4670	87.07	1.21
GAT	0	0.005	5E-5	64	-	8	Full	1525872	2143.036	1105	0.5156	87.01	0.96
GCN2	0	0.005	5E-5	32	-	-	3	48128	256.9575	1708	6.647	83.17	1.50
GCN2	0	0.005	5E-5	32	-	-	10	48128	220.4663	1051	4.7672	84.23	1.57
GCN2	0	0.005	5E-5	32	-	-	Full	48128	210.7702	1302	6.1773	84.38	2.03
GCN2	0	0.005	5E-5	64	-	-	3	100352	353.0055	1581	4.4787	84.70	1.13
GCN2	0	0.005	5E-5	64	-	-	10	100352	300.4794	1021	3.3979	85.01	1.47
GCN2	0	0.005	5E-5	64	-	-	Full	100352	307.7913	1219	3.9605	84.79	1.64
GCN2	0	0.005	5E-5	Input Feature Dim	-	-	3	4117009	3013.6082	1051	0.3488	86.72	1.82
GCN2	0	0.005	5E-5	Input Feature Dim	-	-	10	4117009	3378.9214	925	0.2738	87.66	1.73
GCN2	0	0.005	5E-5	Input Feature Dim	-	-	Full	4117009	3091.4392	1013	0.3277	87.54	1.66

I Empirical Study on Classical Poolings

We study and compare CP pooling with classical pooling methods on Cora on a CPU over 10 runtimes, and compare the number of model parameters, number of training epochs per second, and accuracy. Sampling means we sample '3' neighbors for each node or we use 'Full' neighborhood.

Table 7: Study of Efficiency vs. Performance on Cora. CP pooling in comparison with classical pooling techniques.

	Dropout	LR	Weight Decay	Hidden	Rank	Sampling	#Params	Time(s)	Epoch	Epoch/s	Acc	Std
tGNN	0	0.005	5.00E-05	32	8	3	58128	290.9774	1389	4.7736	85.55	1.33
Mean	0	0.005	5.00E-05	32	-	Full	46080	449.2177	2352	5.2358	83.26	1.06
Mean	0	0.005	5.00E-05	64	-	Full	92160	398.3229	1496	3.7747	83.88	1.77
Max	0	0.005	5.00E-05	32	-	Full	46080	464.0722	2371	5.0655	83.33	1.96
Max	0	0.005	5.00E-05	64	-	Full	92160	394.1546	1496	3.7955	83.68	2.13

J Dataset

A more detailed statistics of real-world datasets.

Table 8: Statistics of node graphs.

Dataset	#Nodes	#Edges	#Node Features	#Edge Features	#Classes
<i>Cora</i>	2,708	5,429	1,433	/	7
<i>Citeseer</i>	3,327	4,732	3,703	/	6
<i>Pubmed</i>	19,717	44,338	500	/	3
<i>PRODUCTS</i>	2,449,029	61,859,140	100	/	47
<i>ARXIV</i>	169,343	1,166,243	128	/	40
<i>PROTEINS</i>	132,534	9,561,252	8	8	112

Table 9: Statistics of graph datasets

Dataset	#Graphs	#Node Features	#Classes
<i>ZINC</i>	12,000	28	/
<i>CIFAR10</i>	60,000	5	10
<i>MNIST</i>	70,000	3	10
<i>MolHIV</i>	41,127	9	2

K Hyperparameter

For experiments on real-world datasets, we use NVIDIA P100 Pascal as our GPU computation resource.

And the searching hyperparameter includes the learning rate, weight decay, dropout, decomposition rank R .

Table 10: Hyperparameter searching range corresponding to Section 6.

Hyperparameter	Searing Range
learning rate	{0.01, 0.001, 0.0001, 0.05, 0.005, 0.0005, 0.003}
weight decay	{5e-5, 5e-4, 5e-3, 1e-5, 1e-4, 1e-3, 0}
dropout	{0, 0.1, 0.3, 0.5, 0.7, 0.8, 0.9}
R	{32, 64, 128, 256, 512, 25, 50, 75, 100, 200}

Table 11: Hyperparameters for tGNN corresponding to Section 6.

Dataset	learning rate	weight decay	dropout	R
<i>Cora</i>	0.001	5.00E-05	0.9	512
<i>Citeseer</i>	0.001	1.00E-04	0	512
<i>Pubmed</i>	0.005	5.00E-04	0.1	512
<i>PRODUCTS</i>	0.001	5.00E-05	0.3	128
<i>ARXIV</i>	0.003	5.00E-05	0	512
<i>PROTEINS</i>	0.0005	5.00E-04	0.9	50
<i>ZINC</i>	0.005	5.00E-04	0	100
<i>CIFAR10</i>	0.005	1.00E-04	0	100
<i>MNIST</i>	0.005	5.00E-05	0	75
<i>MolHIV</i>	0.001	5.00E-05	0.8	100

Checklist

The checklist follows the references. Please read the checklist guidelines carefully for information on how to answer these questions. For each question, change the default **[TODO]** to **[Yes]**, **[No]**, or **[N/A]**. You are strongly encouraged to include a **justification to your answer**, either by referencing the appropriate section of your paper or providing a brief inline description. For example:

- Did you include the license to the code and datasets? **[Yes]** Yes
- Did you include the license to the code and datasets? **[No]** The code and the data are proprietary.
- Did you include the license to the code and datasets? **[N/A]**

Please do not modify the questions and only use the provided macros for your answers. Note that the Checklist section does not count towards the page limit. In your paper, please delete this instructions block and only keep the Checklist section heading above along with the questions/answers below.

1. For all authors...
 - (a) Do the main claims made in the abstract and introduction accurately reflect the paper's contributions and scope? **[Yes]**
 - (b) Did you describe the limitations of your work? **[Yes]**
 - (c) Did you discuss any potential negative societal impacts of your work? **[N/A]**
 - (d) Have you read the ethics review guidelines and ensured that your paper conforms to them? **[Yes]**
2. If you are including theoretical results...
 - (a) Did you state the full set of assumptions of all theoretical results? **[Yes]**
 - (b) Did you include complete proofs of all theoretical results? **[Yes]**
3. If you ran experiments...
 - (a) Did you include the code, data, and instructions needed to reproduce the main experimental results (either in the supplemental material or as a URL)? **[Yes]**
 - (b) Did you specify all the training details (e.g., data splits, hyperparameters, how they were chosen)? **[Yes]**
 - (c) Did you report error bars (e.g., with respect to the random seed after running experiments multiple times)? **[Yes]**
 - (d) Did you include the total amount of compute and the type of resources used (e.g., type of GPUs, internal cluster, or cloud provider)? **[Yes]**
4. If you are using existing assets (e.g., code, data, models) or curating/releasing new assets...
 - (a) If your work uses existing assets, did you cite the creators? **[Yes]**
 - (b) Did you mention the license of the assets? **[Yes]**
 - (c) Did you include any new assets either in the supplemental material or as a URL? **[No]**
 - (d) Did you discuss whether and how consent was obtained from people whose data you're using/curating? **[N/A]**
 - (e) Did you discuss whether the data you are using/curating contains personally identifiable information or offensive content? **[Yes]**
5. If you used crowdsourcing or conducted research with human subjects...
 - (a) Did you include the full text of instructions given to participants and screenshots, if applicable? **[No]**
 - (b) Did you describe any potential participant risks, with links to Institutional Review Board (IRB) approvals, if applicable? **[No]**
 - (c) Did you include the estimated hourly wage paid to participants and the total amount spent on participant compensation? **[No]**